Pharm Res (2012) 29:1843–1853
DOI 10.1007/s11095-012-0708-6

RESEARCH PAPER

Fluorescence Imaging of the Lymph Node Uptake of Proteins in Mice after Subcutaneous Injection: Molecular Weight Dependence

Fang Wu • Suraj G. Bhansali • Wing Cheung Law • Earl J. Bergey • Paras N. Prasad • Marilyn E. Morris

Received: 20 November 2011 / Accepted: 10 February 2012 / Published online: 29 February 2012

ABSTRACT

Purpose To use noninvasive fluorescence imaging to investigate the influence of molecular weight (MW) of proteins on the rate of loss from a subcutaneous (SC) injection site and subsequent uptake by the draining lymph nodes in mice.

Methods Bevacizumab (149 kDa), bovine serum albumin (BSA, 66 kDa), ovalbumin (44.3 kDa) or VEGF-C156S (23 kDa), labeled with the near infrared dye IRDye 680, were injected SC into the front footpad of SKH-1 mice. Whole body non-invasive fluorescence imaging was performed to quantitate the fluorescence signal at the injection site and in axillary lymph nodes.

Results The half-life values, describing the times for 50% loss of proteins from the injection site, were 6.81 h for bevacizumab, 2.85 h for BSA, 1.57 h for ovalbumin and 0.31 h for VEGF-C156S. The corresponding axillary lymph node exposure, represented as the area of the % dose *versus* time curve, was 6.27, 5.13, 4.06 and 1.54% dose · h, respectively.

Conclusions Our results indicate that the rate of loss of proteins from a SC injection site is inversely related to MW of proteins, while lymph node exposure is proportionally related to the MW of proteins in a mouse model.

KEY WORDS fluorescence imaging · lymphatic uptake · molecular weight · protein · subcutaneous injection

ABBREVIATIONS

BSA	bovine serum albumin
F_{LN}	fraction of the dose recovered at the axillary lymph nodes
F_{SC}	fraction of original signal remaining at the SC injection site
IRDye	infrared dye
LN	lymph node
MW	molecular weight
ROI	region of interest
SC	subcutaneous
SDS-PAGE	sodium dodecyl sulfate-polyacrylamide gel electrophoresis
VEGF	vascular endothelial growth factor

INTRODUCTION

Subcutaneous (SC) administration continues to be an important route for the delivery of protein drugs. Following SC administration, a drug can be transported to the blood system either by the blood capillaries or by the lymphatics. While small drug molecules are rapidly and extensively absorbed after SC injection, the systemic bioavailability of protein drugs is often incomplete with values ranging from ~20 to 100% of the administered dose (1,2). One of the reasons is that, for small molecules, the blood capillary wall diffusivity is very high and there is little restriction to drug transport, whereas the permeability of macromolecules through the blood capillaries is low (3,4). Based on studies performed using a sheep model, the lymphatics have been reported to represent the primary absorptive pathway for molecules with molecular weights (MW) greater than

F. Wu · S. G. Bhansali · M. E. Morris (✉)
Department of Pharmaceutical Sciences
School of Pharmacy and Pharmaceutical Sciences
University at Buffalo, State University of New York
517 Hochstetter Hall
Amherst, New York 14260, USA
e-mail: memorris@buffalo.edu

W. C. Law · E. J. Bergey · P. N. Prasad
Institute for Lasers, Photonics and Biophotonics
University at Buffalo, State University of New York
Amherst, New York 14260, USA

Present Address:
S. G. Bhansali
Novartis Pharmaceuticals Corporation, Clinical PKPD
East Hanover, New Jersey 07936, USA

16 kDa since more than 50% of the administered dose is recovered in peripheral lymph for these proteins (3). If the protein drugs are not removed or degraded during transport through the lymphatic system, proteins enter the bloodstream via the thoracic and right lymphatic ducts, contributing to the bioavailability of the proteins.

Studies in the sheep model have demonstrated a linear relationship between the MW of a protein and the proportion of the dose absorbed by the lymphatics, as determined by popliteal lymph sampling following the SC administration of proteins (3). A similar relationship has been demonstrated in the rat, although the amounts of proteins recovered in the thoracic lymph were small (5).

The objective of this study was to evaluate the influence of MW on the absorption of protein from an SC injection site and draining lymph node uptake of a series of proteins following SC administration in mice using *in vivo* optical imaging. We labeled four proteins with different MWs, namely bevacizumab (149 kDa), bovine serum albumin (BSA) (66 kDa), ovalbumin (44.3 kDa) and VEGF-C156S (23 kDa), with a near infrared dye, IRDye 680. To overcome the difficulties of lymph sampling from small animals, noninvasive real time fluorescent imaging of the live mice was performed to quantitatively evaluate the loss of protein-IRDye 680 conjugates from the SC injection site and their accumulation over time in the axillary lymph nodes that drain the site of SC injection. The use of proteins of varying MWs allows the exploration of the role of MW in the absorption rate and the lymphatic uptake of the proteins.

MATERIALS AND METHODS

Materials

IRDye 680 protein labeling-High MW kit was purchased from LI-COR Biosciences (Lincoln, NE, USA). Avastin® (bevacizumab, 25 mg/mL; Genentech) was purchased from Genentech (San Francisco, CA, USA). Bovine serum albumin (BSA, purity ≥99%) and ovalbumin (not less than 98% pure) were obtained from Sigma-Aldrich (St. Louis, MO, USA). Recombinant human VEGF-C (Cys156Ser), purity >95%, was purchased from R&D Systems (Minneapolis, MN, USA). Novex tris-glycine SDS sample buffer, NuPAGE® sample reducing agent, Novex tris-glycine-SDS running buffer, Novex 10% tris-glycine gel for sodium dodecyl sulfate-polyacrylamide gel electrophoresis (SDS-PAGE) for high molecular weight proteins (>30 kDa) and Novex tricine SDS sample buffer, Tris-tricine-SDS running buffer, Novex 16% tricine gel for SDS-PAGE for low molecular weight proteins (<30 kDa) and Novex sharp protein standard and SimplyBlue® safe stain were purchased from Invitrogen (Carlsbad, CA, USA). Isoflurane was obtained from Hospira Inc. (Lake Forest, IL, USA). Pierce Zeba™ desalting spin column was obtained from Pierce Biotechnology (Rockford, IL, USA).

Synthesis of IRDye-680-Labeled Protein Conjugates

Using an IRDye 680 protein labeling kit, 1 mg of bevacizumab, BSA, or ovalbumin or 100 μg of VEGF-C156S was conjugated with IRDye 680 according to the manufacturer's instructions. For example, for ovalbumin, the pH of 1 mL of 1 mg/mL ovalbumin in PBS solution was adjusted to 8.5 by adding 0.1 mL of 1 M potassium phosphate buffer (pH 9). Then 21.4 μL of 4.2 mM IRDye 680-NHS ester in water was added drop by drop into the above ovalbumin solution and the solution was kept at room temperature for 2 h in the dark without stirring. The reaction molar ratio of IRDye 680 to ovalbumin was 4:1. After the conjugation, the reaction solution was then loaded on a Pierce Zeba™ desalting spin column and centrifuged at 1,000×*g* for 2 min to remove the free dye. The ovalbumin-IRDye 680 conjugate was stored at −20°C until use. The other protein-IRDye 680 conjugates were synthesized using a similar procedure. The concentration of each protein in PBS solution used in the conjugation reaction was 1 mg/mL. The reaction molar ratios of IRDye 680 to bevacizumab, BSA and VEGF-C156S were 8:1, 4:1 and 15:1, respectively, which were optimized based on the reaction conditions suggested by the IRDye manufacturer.

To calculate the dye and protein labeling ratio (dye over protein ratio, D/P) for the IRDye 680 labeled protein conjugates, the BSA, ovalbumin and VEGF-C156S conjugates were diluted with PBS: methanol (1:1). Bevacizumab conjugates were diluted with PBS: methanol (9:1). A UV-visible spectrophotometer PharmaSpec UV-1700 (Shimadzu Scientific Instruments, Columbia, MD, USA) was used to determine the molar extinction coefficient at 280 nm of proteins (ε protein) and the absorbance of the protein IRDye 680 conjugates at 280 nm (A280) and 688 nm (A688). The D/P ratio was calculated according to the absorbance of the IRDye 680 at 688 nm and the absorbance of proteins at 280 nm based on the manufacturer's instructions (LI-COR). The final bevacizumab, BSA, ovalbumin or VEGF-C156S concentrations were calculated according to the absorbance of protein conjugates at 280 nm.

Confirmation of the IRDye-680-Labeled Protein Conjugates by SDS-PAGE

Reducing SDS–PAGE was performed to confirm the conjugation of the proteins with IRDye 680 using an XCell SureLock™ Mini-Cell electrophoresis system (Invitrogen, Carlsbad, CA). For bevacizumab, BSA and ovalbumin IRDye 680 conjugates, 8 μL of each conjugate was mixed with 10 μL of Novex Tris-Glycine SDS sample buffer and

2 μL of NuPAGE sample reducing agent and separated on a 10% Tris-Glycine gel. Electrophoresis for the above three proteins was carried out at a constant voltage (200 V) for 40 min. VEGF-C156S conjugates or standards were mixed with Novex Tricine SDS sample buffer and reducing agent and separated on a Novex 16% Tricine gel. Electrophoresis for VEGF-C156S was carried out at a constant voltage (200 V) for 26 min. After taking fluorescent images with the Maestro *in vivo* imaging system (Cambridge Research & Instrumentation, Inc., Woburn, MA) with an excitation wavelength of 575–605 nm and emission wavelength of 645 nm long pass using an exposure time of 1000 ms, the gels were stained with SimplyBlue® safe stain overnight and then imaged with Maestro imaging system using white light.

Non-Invasive Fluorescence Imaging

For non-invasive fluorescence imaging, 8 to 12 week-old male immunocompetent, hairless SKH-1 mice (Charles River Laboratories, Wilmington, MA) were used (6). All mice were maintained and used in accordance with the animal protocol approved by the Institutional Animal Care and Use Committee, University at Buffalo. SKH-1 mice were injected subcutaneously in the right front footpad (Fig. 1) with 0.1 mg/kg of IRDye 680 labeled bevacizumab, 0.1 mg/kg of IRDye 680 labeled BSA, 0.08 mg/kg of IRDye 680 labeled ovalbumin or 0.01 mg/kg of IRDye 680 labeled VEGF-C156S (the injection volume for each protein is about 15 μL). The doses of the dye of the above four protein conjugates are all equivalent to 1.5 nmol IRDye 680/kg. We selected this dye dose because preliminary studies with varying doses indicated no saturation of the fluorescence signal at this dose. Non-invasive fluorescence imaging of the SC injection site and lymph nodes that drain the SC injection site (Fig. 1) was carried out using the Maestro imaging system (7–10). A filter set with the excitation wavelength of 575–605 nm and emission wavelength of 645 nm long pass was used for acquiring fluorescence imaging of protein-IRDye 680 conjugate *in vivo*. Identical imaging conditions, including exposure time (1 s), binning factor (2×2), and fields of view (5.0×6.8 cm), were used for acquiring all images. Animals were anesthetized with isoflurane and placed dorsally in the Maestro imaging system, and images were taken at 5, 10, 15 and 30 min and 1, 2, 3, 4, 5, 8 and 24 h. The injection site was covered with black tape to avoid saturation of the camera by the strong fluorescence signal at the injection site (11). The captured images (spectral cube, containing a spectrum at every pixel) were analyzed using the Maestro software. Spectra from the autofluorescence from the skin and IRDye 680 associated fluorescence signal were unmixed and the background was subtracted. Then the fluorescence signal at the region of interest (ROI) was quantitatively analyzed using the software. The axillary lymph nodes area and the injection site were designated as the two ROIs. The fraction of the dose present at the SC injection site (F_{SC}%) was determined by dividing the fluorescence signal at the ROI of the SC injection site at predetermined time points by the maximal fluorescence signal at the ROI of the SC injection site, which was assumed to represent the injected dose. Then F_{SC}% was plotted as a function of time. The fraction of the dose recovered in the axillary lymph nodes (F_{LN}%) was determined by dividing the total fluorescence signal at the ROI of the axillary lymph nodes at each time point by the maximal fluorescent signal at the ROI of the injection site and plotted as a function of time.

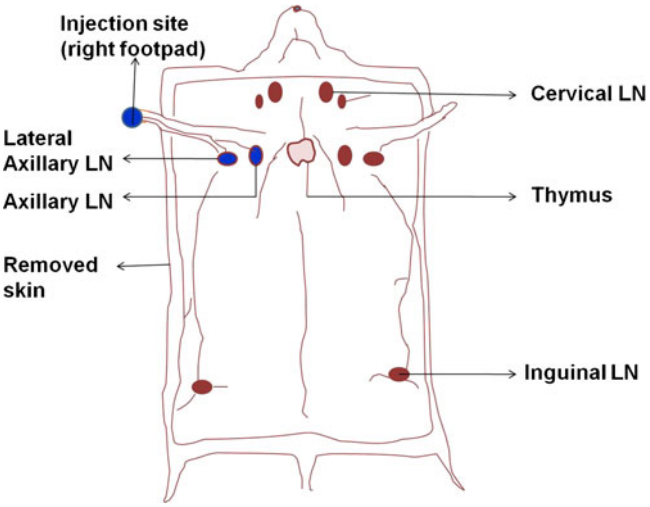

Fig. 1 Schematic of the route of SC injection and the uptake of protein-IRDye 680 conjugate in the axillary lymph nodes including lateral axillary lymph node and axillary lymph node in our mouse model. The site of injection and localization of lateral axillary lymph node (LN), axillary lymph node, cervical lymph nodes, inguinal lymph nodes and thymus are indicated.

Characterization of the Stability of IRDye-680-Labeled Protein in Lymph Node Homogenate and Injection Site Homogenate

Stability of IRDye-680 labeled bevacizumab, BSA and ovalbumin was determined in lymph node homogenates and injection site homogenate using SDS-PAGE. Blank lymph nodes and injection site tissues including skin and fat were homogenized in T-PER tissue protein extraction reagent (20:1, v/w (mL:g)). IRDye 680 protein conjugates (500 μg/mL) were incubated in lymph node homogenate or injection site homogenate at 37°C for 0, 24 and 72 h. An aliquot (8 μL) of each sample was mixed with 12 μL of Laemmli Sample Buffer with 5% β-mercaptoethanol and 10 μL of each sample was separated on a 4%–15% precast polyacrylamide gel (BIO-RAD, Hercules, CA). Electrophoresis for the above three proteins was carried out at a constant voltage (200 V) for about 25 min.

Data Analysis

In order to better characterize the loss of different proteins from the SC injection site, nonlinear regression was performed for the mean value of F_{SC}% *versus* time plots using GraphPad Prism (v. 5.0, GraphPad Software, San Diego, California, USA). The fitting model is $Fsc = Fsc0 \bullet \exp(-k * t)$, where Fsc0 is the Fsc value when t (time) is zero and k is the rate constant for the loss from the SC injection site. Half-life ($t_{1/2}$), representing 50% loss from the SC injection site, was calculated as ln(2)/k. For the four F_{LN}% *versus* time profiles, non-compartmental analysis was performed using WinNonlin 5.0 (Pharsight Corporation, Mountain View, CA, USA). The maximum F_{LN}% (F_{max}) and time to reach the maximum (t_{max}) were calculated directly from experimental data (n=3). The area under the F_{LN}% *versus* time curve from zero to infinity ($AUC_{0-\infty}$) was calculated by the trapezoidal rule with extrapolation to infinity based on the value of F_{LN}% *versus* time plots.

RESULTS

Synthesis and Characterization of Protein IRDye 680 Conjugates

In our study, we employed the fluorescent dye, IRDye 680 which bears an NHS ester reactive group that is coupled to the primary amines of bevacizumab, BSA, ovalbumin and VEGF-C156S, forming stable bioconjugates. The D/P ratios of IRDye 680 to bevacizumab, BSA, ovalbumin and VEGF-C156S were 2:1, 1:1, 0.9:1 and 4:1, respectively, when the reaction molar ratios of IRDye 680 to bevacizumab, BSA, ovalbumin and VEGF-C156S were 8:1, 4:1, 4:1 and 15:1, respectively. The final concentration of bevacizumab, BSA, ovalbumin or VEGF-C156S was measured as 0.88, 1.08, 1.23 and 0.75 mg/mL, respectively. This is close to the original concentration of proteins (1 mg/mL) used in the synthesis reaction, indicating that the conjugate purification process by the desalting spin column did not result in significant loss of the proteins.

Confirmation of the IRDye-680-Labeled Proteins by SDS-PAGE

Following purification, the IRDye680 conjugated proteins were analyzed by SDS-PAGE to confirm the conjugation of dye and proteins. Prior to staining with SimplyBlue®, containing Coomassie Blue, the gel was illuminated using the Maestro customized filter set with the excitation wavelength of 575–605 nm and the emission wavelength of 645 nm long pass to detect any fluorescence arising from IRDye 680 conjugated protein bands. As shown in Fig. 2a, two clear single bands of bevacizumab-IRDye 680 conjugate were detected by both SimplyBlue® staining (Fig. 2a, right panel) and fluorescence imaging (Fig. 2a, left panel), while the two bands of bevacizumab standard were only visible by SimplyBlue® staining (Fig. 2a, right panel). Antibodies under reduced SDS-PAGE conditions produce heavy chains and light chains since the disulphide bonds are cleaved following treatment with reducing reagents (12). Therefore, the two bands shown in each column on the right panel of Fig. 2a correspond to the heavy chains (~50 kDa) and light chains (~25 kDa) of bevacizumab. The SDS-PAGE results indicated that bevacizumab was successfully conjugated with IRDye 680 without any degradation. Similarly, SDS-PAGE results of BSA, ovalbumin and VEGF-C156S also confirmed the successful conjugation of these proteins with IRDye 680 (Fig. 2b–d). The two bands shown in each column on the right panel of Fig. 2c correspond to the two N-linked glycan structural isomers of ovalbumin (13).

Real-Time Non-Invasive Dynamic Imaging

In this study, doses of the four protein conjugates, containing equimolar doses of the IRDye 680 were injected SC into the front footpad of SKH-1 mice. Spectra from the autofluorescence from the skin of SKH-1 mouse (coded red) and protein-IRDye 680 associated fluorescence signals (coded blue) were unmixed using the Maestro software, as shown in Fig. 3a–d. As shown in Fig. 4, images a–j correspond to representative fluorescence images after SC injection of bevacizumab-IRDye 680 conjugate into the right front footpad of a SKH-1 mouse, where the fluorescence signal in the mouse is shown in white. The images B–J were used for the quantification of the fluorescence signal at the ROI of the axillary lymph nodes and image A and other similar images (not shown) taken at predetermined time points were used for the quantification of the fluorescence signal at the ROI of the injection site. As seen from Fig. 4b, the fluorescent signal was detected from the axillary lymph nodes 5 min after the injection of bevacizumab-IRDye 680, suggesting the rapid uptake of bevacizumab by the draining lymph nodes. The fluorescence intensity gradually increased, reaching the maximum at about 3 h post injection (Fig. 4g). The fluorescence intensity then gradually decreased, indicating the clearance of the bevacizumab-IRDye 680 from the axillary lymph nodes. Similar data were collected for BSA-IRDye 680, ovalbumin-IRDye 680 and VEGF-C156S-IRDye 680 conjugates (image data not shown).

Ex Vivo Optical Imaging of Dissected Lymph Nodes and Thymus

To confirm the uptake of IRDye 680-protein conjugates by the draining lymph nodes, lymph nodes and thymus were

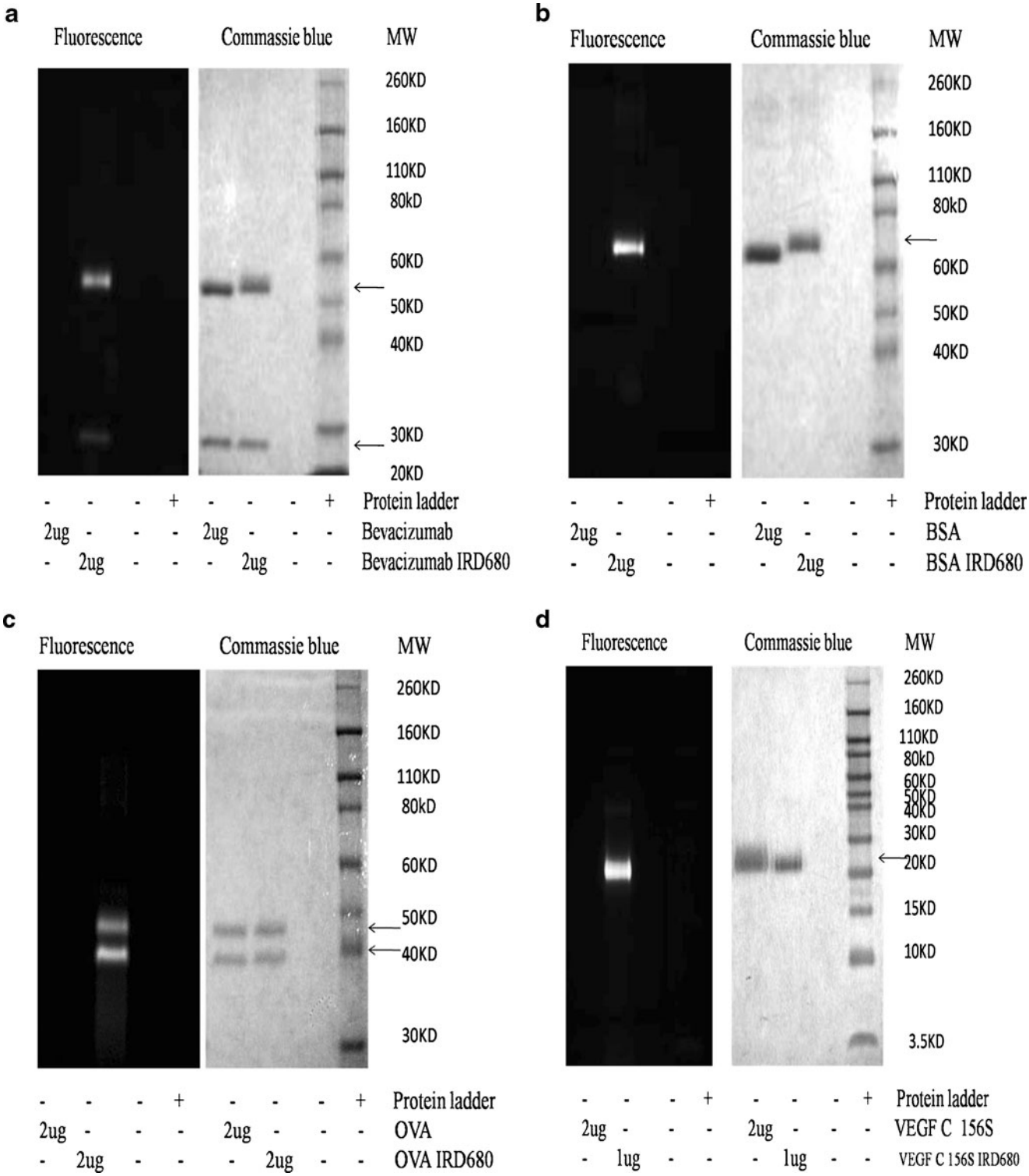

Fig. 2 Sodium dodecyl sulfate polyacrylamide gel electrophoresis (SDS-PAGE) of dye-conjugated and control proteins, (**a**) bevacizumab, (**b**) BSA, (**c**) ovalbumin, (**d**) VEGF-C156S, with detection by both Coomassie Blue staining (right panel) and fluorescence imaging (left panel).

harvested 1 h post-SC injection for the 4 IRDye 680 labeled proteins. For all of the 4 protein IRDye 680 conjugates, the fluorescent signal could be detected in the axillary lymph nodes on the injection side, but not in those present on the non-injection side. No fluorescence signal was detected from the cervical or inguinal lymph nodes on either the injection side or non-injection side. The results confirm that the proteins were only present in the axillary lymph nodes

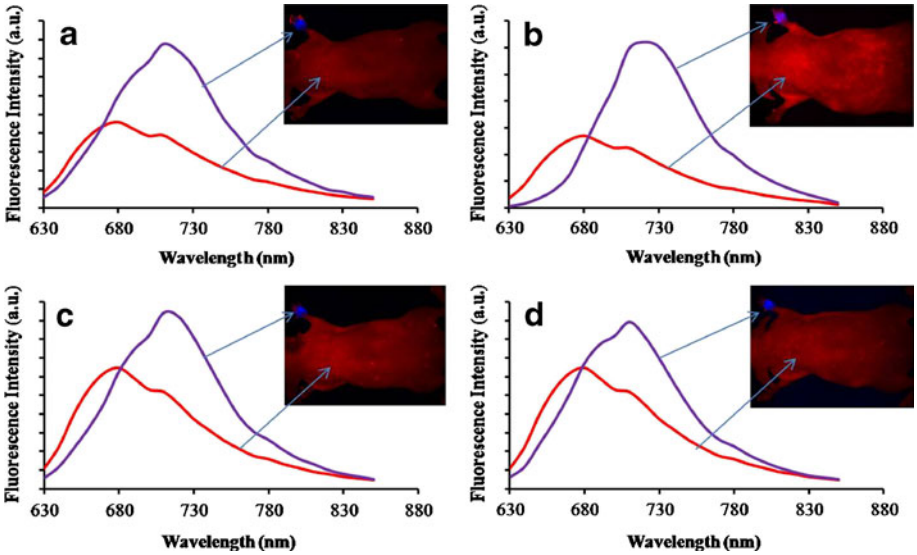

Fig. 3 Spectra of autofluorescence (red) and protein-IRDye 680 conjugate (blue) from a SKH-1 mouse after SC injection of bevacizumab-IRDye 680 conjugate (**a**), BSA-IRDye 680 conjugate (**b**), ovalbumin-IRDye 680 conjugate (**c**) or VEGF-C156S-IRDye 680 conjugate (**d**) in the front footpad of SKH-1 mouse. The mice are placed in a dorsal position in this figure.

post-SC injection for all 4 protein IRDye 680 conjugates. *Ex vivo* optical imaging of dissected lymph nodes and thymus also indicated that redistribution of these proteins from blood into lymph nodes does not occur to a significant degree.

Stability of Fluorescent Signal and Conjugate in Lymph Node and Injection Site Homogenates

The SDS-PAGE analysis of BSA-IRDye 680 conjugate in lymph node homogenate and injection site homogenate after incubation for 0, 24 and 72 h at 37°C (Fig. 5a and b) showed that BSA remained as a single band for as long as 72 h. The total fluorescence was still associated with BSA and there were minimal degradation products of lower molecular weights shown on the gel. Image J software (National Institute of Health, Bethesda, Maryland, USA) was used to quantitatively measure the fluorescence signal from the BSA band. When the fluorescence signal of BSA band for the 0 h sample was set as 100%, the average fluorescence signals associated with BSA band for 24 hour-sample of the

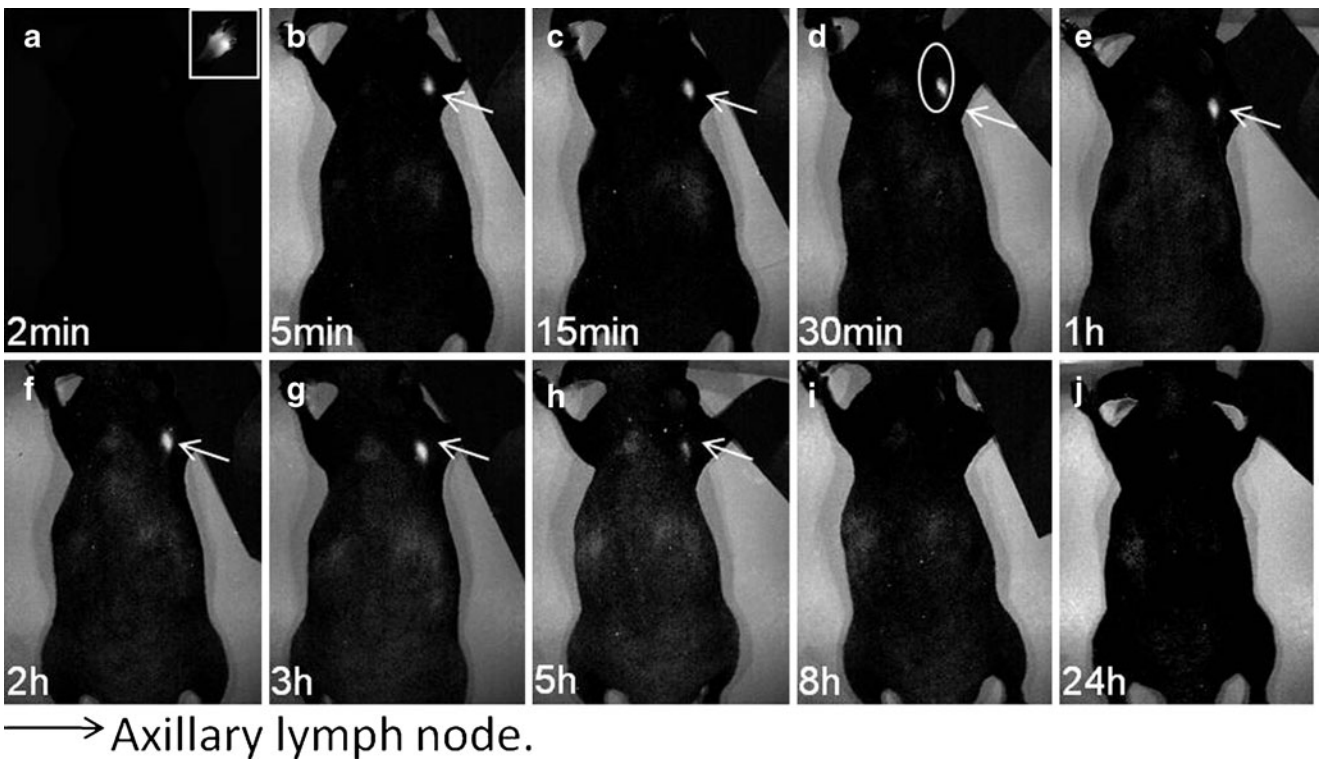

Fig. 4 Representative images of SKH-1 hairless mice after SC injection of 0.1 mg/kg of bevacizumab-IRDye 680 (D/P=2:1) in the front footpad. The ROI of the axillary lymph node is indicated by a circle and the ROI of the SC injection site is indicated by a square. White arrows indicate axillary lymph nodes.

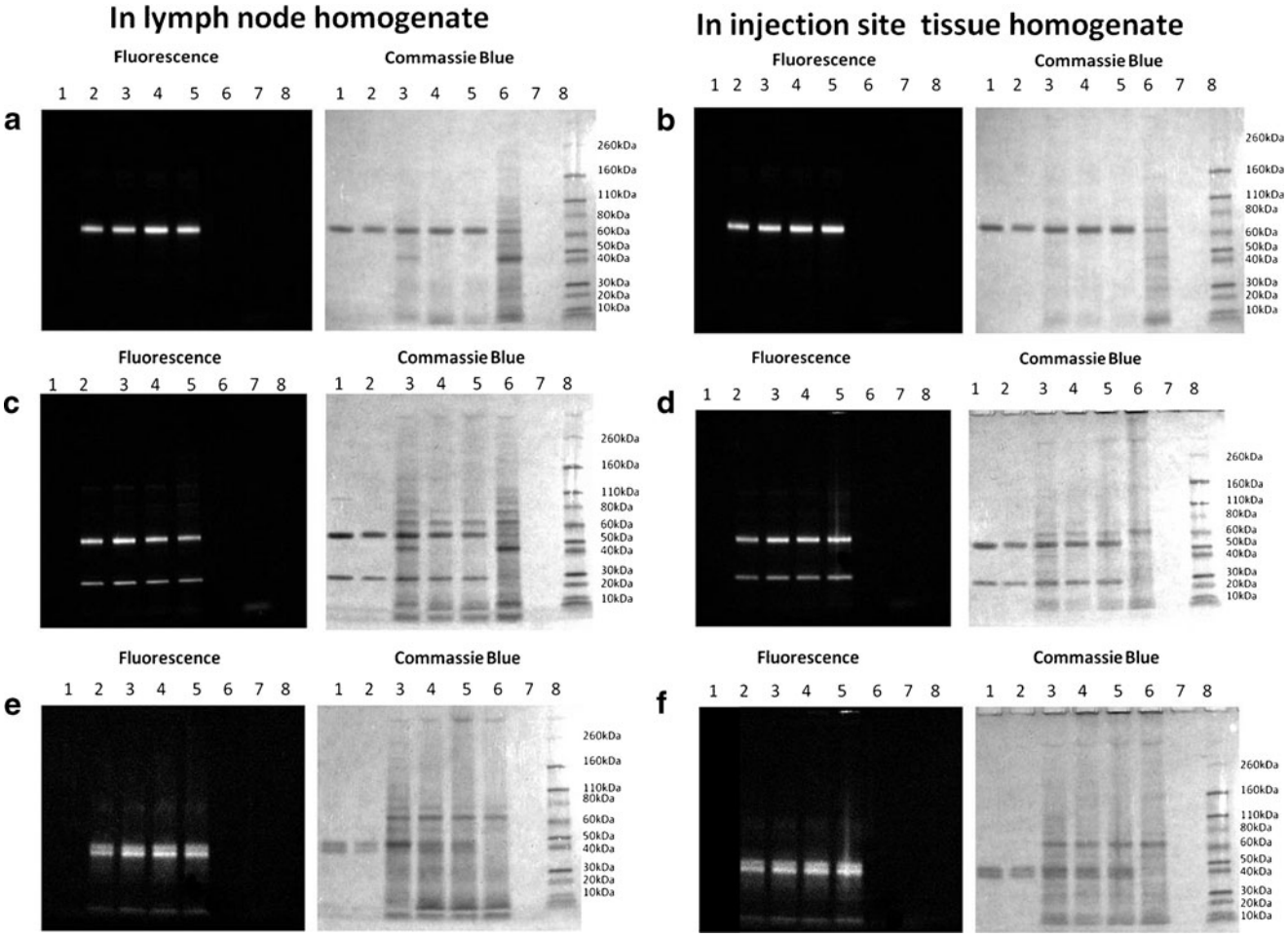

Fig. 5 Characterization of stability of protein-IRDye 680 conjugates. (**a**, **b** for BSA; **c**, **d** for Bevacizumab; **e**, **f** for ovalbumin) a, c, e Sodium dodecyl sulfate polyacrylamide gel electrophoresis (SDS-PAGE) of (*1*) 2 μg of protein in PBS, (*2*) 2 μg of protein-IRDye 680, (*3*,*4*,*5*) 2 μg of protein-IRDye 680 conjugate standard and protein-IRDye 680 conjugate after incubation in lymph node homogenate at 37°C for 0, 24 and 72 h. (*6*) blank lymph node homogenate, (*7*) free IRDye 680, (*8*) MW marker. b, d, f. SDS-PAGE of (*1*) 2 μg of protein in PBS, (*2*) 2 μg of protein-IRDye 680, (*3*,*4*,*5*) 2 μg of protein-IRDye 680 conjugate standard and protein-IRDye 680 conjugate after incubation in injection site homogenate at 37°C for 0, 24 and 72 h. (*6*) blank injection site tissue homogenate, (*7*) free IRDye 680, (*8*) MW marker. Protein-IRDye680 conjugate was detected by both Coomassie Blue staining (right panel) and fluorescence imaging (left panel).

injection site tissue homogenate and the lymph node homogenate are 114±1.77% and 119±1.68% (n=3), respectively. This indicated that the decrease in fluorescence over time observed for BSA-IRDye 680 in the axillary lymph nodes and injection site is not due to quenching of the fluorescence label or loss of free label from the BSA-IRDye 680 conjugate. Thus, SDS-PAGE results suggest that the fluorescence detected in the lymph nodes and injection site within 24 h during the non-invasive imaging study would represent intact BSA. These results with BSA were confirmed in studies using size exclusion HPLC, where neither free dye nor fluorescent-labeled breakdown products of BSA were detected (data not presented). Similar results regarding stability in lymph node homogenates have been obtained using bevacizumab-IRDye 680 and ovalbumin-IRDye 680 (Fig 5c and e). For the injection site tissue homogenate studies, bevacizumab-IRDye 680 and ovalbumin-IRDye 680 showed predominantly protein bands on the gel for as long as 72 h (Fig 5d and f). The fluorescence signals associated with heavy chain band of bevacizumab-680 after a 24 hour-incubation in the injection site tissue homogenate and in the lymph node homogenate were 100.2±2.02% and 83.4±1.38% (n=3) of that of original control sample (time 0), respectively. The fluorescence signals associated with two isoforms of ovalbumin-680 after a 24 hour-incubation in the injection site tissue homogenate and in the lymph node homogenate were 113.2±2.09% and 104.3±2.90% (n=3), respectively. Our results indicate that there is limited signal quenching or loss of free dye after incubation for 24 h in injection site tissue homogenate or lymph node homogenate when compared with the original control sample. Thus the fluorescence signals obtained at the injection site and in axillary lymph nodes after SC administration of bevacizumab, BSA, ovalbumin conjugate

during the non-invasive imaging suggest that the proteins remain intact and associated with the fluorescent label. Similar studies were not performed for VEGF-C156S due to the cost and availability of the protein, but previous work using ^{125}I VEGF-C156S demonstrated good stability of the radiolabeled protein when incubated in buffer at 37°C for 72 h, and complete bioavailability after SC injection (14). *In vivo* experiments may need to be performed to further confirm the above stability result because tissue homogenates may not metabolize proteins as efficiently as whole organs *in vivo*.

Loss from the SC Site and Uptake by Lymph Nodes: Relationships with MW

After SC injection of the four protein-IRDye 680 conjugates, the percentage of injected dose remaining at the injection site (F_{SC}%) was determined and plotted as a function of time (Fig. 6a). A linear relationship between the rate of the loss of proteins from the injection site and the MW of proteins was observed. The loss of the IRDye 680 labeled bevacizumab with the highest MW (149 kDa) from the injection site was the slowest, followed by BSA (66 kDa) and ovalbumin (44.3 kDa). The IRDye 680 labeled VEGF-C156S with the smallest MW of 23 kDa was cleared from the injection site the fastest. Nonlinear regression was performed for the mean F_{SC}% value *versus* time plot using GraphPad Prism software. The $t_{1/2}$, representing time for 50% loss of protein from the injection site was 6.81 h for bevacizumab-IRDye 680, 2.85 h for BSA-IRDye 680, 1.57 h ovalbumin-IRDye 680- and 0.31 h for VEGF-C 156S-IRDye 680. There was a linear relationship between half-life and molecular weight (R^2=0.997) (Fig. 6b).

Based on the quantification of the total fluorescence signal at the axillary lymph nodes and the maximum fluorescence signal at the injection site, the fraction of the injected dose recovered in the axillary lymph nodes (F_{LN}%) was calculated (Fig. 7). The longest time to reach maximum amounts of protein conjugates in the axillary lymph nodes (t_{max}) occurred with bevacizumab-IRDye 680 (Table I). The AUC values from time zero to infinity for the axillary lymph nodes were calculated as 6.27±3.08, 5.13±1.81, 4.06±2.06 and 1.54±1.09% dose · h for IRDye680 labeled bevacizumab (149 kDa), BSA (66 kDa), ovalbumin (44.3 kDa) and VEGF-C156S (23 kDa), respectively. The AUC, representing the total lymphatic exposure at the site of axillary lymph nodes of the proteins after SC administration, was found to be proportionally related to their MW within this MW range.

DISCUSSION

Subcutaneous administration represents an important route of delivery for protein-based drugs because of the relative ease of administration and improved patient compliance and quality of life. Normally, small molecules (<2,000 Da) are predominantly cleared by uptake from a subcutaneous injection site into the blood capillaries, whereas particulates and molecules of increasing molecular size have restricted uptake into blood capillaries, instead being absorbed into the lymph capillaries (15). However, very little is known about the factors that govern the absorption of proteins after SC administration and the resulting impact of these processes on the bioavailability and pharmacokinetic

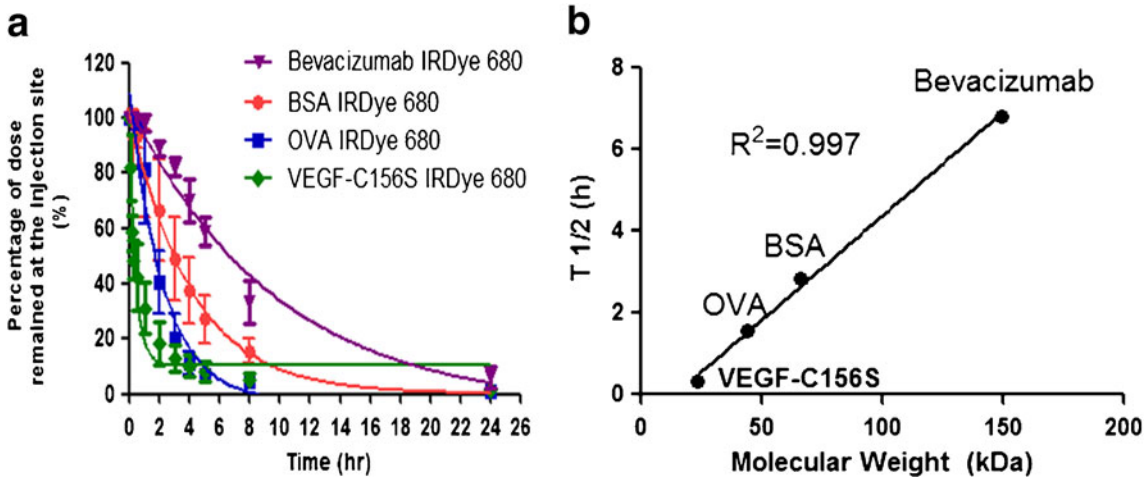

Fig. 6 (**a**) Percentage of dose of proteins remaining at the SC injection site, F_{SC} (%), after SC injection of 0.1 mg/kg of bevacizumab-IRDye 680 conjugate, 0.1 mg/kg of BSA-IRDye 680 conjugate, 0.08 mg/kg of ovalbumin-IRDye 680 conjugate or 0.01 mg/kg of VEGF-C156S-IRDye 680 conjugate (with the doses of the dye all equivalent to 1.5 nmol IRDye 680/kg) in the front footpad of SKH-1 hairless mice (n=3). (**b**) Relationship between MW and half life representing 50% loss from the SC injection site for the four IRDye 680-protein conjugates. Linear regression analysis resulted in a correlation coefficient (r^2) of 0.997 ($p<0.01$).

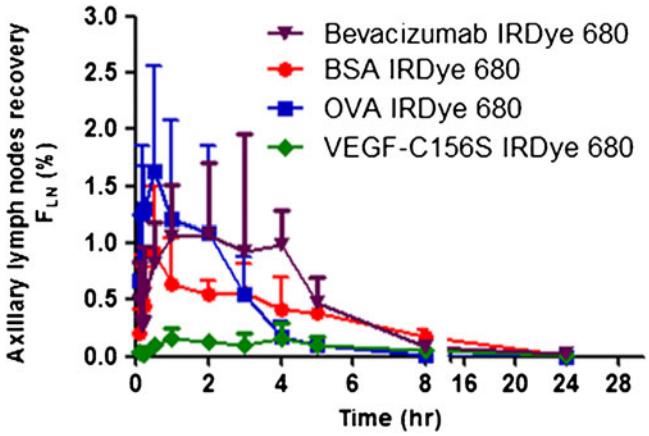

Fig.7 Axillary lymph nodes exposure, F_{LN} (%), after SC injection of 0.1 mg/kg of bevacizumab-IRDye 680 conjugate, 0.1 mg/kg of BSA-IRDye 680 conjugate, 0.08 mg/kg of ovalbumin-IRDye 680 conjugate or 0.01 mg/kg of VEGF-C156S-IRDye 680 conjugate (with the doses of the dye all equivalent to 1.5 nmol IRDye 680/kg) in the front footpad of SKH-1 hairless mice (n=3).

profiles of proteins, especially in a murine model. This could be due to the difficulties and complexity of lymph sampling from small animals, which have been described by Kagan *et al.* (5).

In this study, we developed a novel non-invasive fluorescence imaging method which could provide a convenient method to quantitatively compare the draining lymph node uptake of proteins with different MW or other physicochemical or formulation properties. The main advantages of optical imaging lie in its high resolution and its ability to image at a molecular level (16). Optical imaging has been used in image guided drug/protein delivery (17–20), lymph node imaging (21–23) and tumor targeting in animal models (7,8,24–26). It has also been used in pharmacokinetic/pharmacodynamic studies (27,28), for determining disease progression (29) and investigating drug biodistribution and therapeutic effects from the molecular to organ levels (27, 30,31). The main disadvantage of optical imaging is the poor depth sensitivity of the technique, and penetration beyond 1–2 cm is currently unrealistic (32). However, using near infrared fluorochromes, whose emission wavelength falls in the "window of transparency" between 700 and 900 nm, will maximize tissue penetration and minimize auto-fluorescence (10,11,33–35). Therefore, we have used four proteins conjugated with a near-infrared dye IRDye 680 with emission at 707 nm to evaluate the lymph node uptake of fluorescent labeled proteins in a SKH-1 hairless mouse model using non-invasive fluorescence imaging of lymph nodes that drain the SC site of injection. For lymph nodes present in the periphery, such as the brachial and axillary lymph nodes draining the forearm, it has been reported that all afferent lymph vessels will release lymph into the draining lymph nodes and efferent lymph vessels will carry lymph away (36,37). However, if all lymph does not drain through the axillary lymph nodes, then our protein determination will represent an underestimation of the amount of protein absorbed through the lymphatic system.

Our results are consistent with the findings of previous studies in sheep showing that an inverse relationship between the rate of disappearance of radiolabeled insulin analogues from the SC injection site and the average effective size of insulin and its analogues (38,39). Further *in vivo* studies from our group have found that the bioavailability of VEGF-C156S (14), BSA, and bevacizumab (Wu F and Morris ME, unpublished data) after SC administration in mice is excellent. The bioavailability is complete for VEGF-C156S and bevacizumab, and 88% for BSA after SC administration in a mouse model, indicating that there is little loss due to degradation of these proteins at the SC site. Therefore, with the assumption that the disappearance rate from the injection site equals the combined rate of absorption into the blood and lymphatics, we can infer that MW of proteins is inversely related to the rate of their absorption. We also demonstrated that MW is proportionally related to the lymph node exposure to proteins within a given MW range (23–149 kDa). This is consistent with the results obtained from the sheep model that demonstrated a linear relationship between the MW of proteins and the proportion of the dose absorbed by the lymphatic system (3), as well as in rats (5).

In examining the relationship between lymphatic absorption and bioavailability, Charman *et al.* (40) indicated from studies in a sheep model that lymphatic absorption contributed significantly to the overall insulin bioavailability following SC administration. In a swine model, Harvey *et al.* (41)

Table I PK Parameters for Axillary Lymph Node Exposure (F_{LN}%) of Four Protein IRDye 680 Conjugates

Parameter	Bevacizumab-IRDye 680 (149 kDa)	BSA-IRDye 680 (66 kDa)	Ovalbumin-IRDye 680 (44.3 kDa)	VEGF-C156S-IRDye 680 (23 kDa)
t_{max} (h)	2.67 ± 1.53	1.17 ± 0.76	0.42 ± 0.14	0.83 ± 0.29
F_{max} (% dose)	1.40 ± 0.67	1.07 ± 0.39	1.82 ± 0.84	0.18 ± 0.06
AUC $_{0-\infty}$ (% dose*h)	6.27 ± 3.08	5.13 ± 1.81	4.06 ± 2.06	1.54 ± 1.09

The maximum F_{LN}% (F_{max}) and time to reach the maximum (t_{max}) were calculated directly from experimental data (n=3). Noncompartmental analysis was performed using WinNonlin to calculate AUC $_{0-\infty}$ based on the value of F_{LN}% *versus* time plots

also demonstrated that lymphatic absorption may be a significant contributor of systemic uptake from microneedle intradermal (ID) delivery of protein. In our mouse model, using non-invasive fluorescence imaging, the axillary lymph nodes' exposure is low, but is proportionally related to the MW of proteins after their SC administration.

Understanding of the relationship between the MW of proteins and the absorption rate and extent of draining lymph node uptake is of critical importance in terms of optimizing targeting properties and increasing bioavailability. The lymphatics also represent a target for immunomodulatory agents, vaccines, and anti-metastatic chemotherapeutic compounds, and optimization of lymphatic transport may prove beneficial for such therapeutic agents. The non-invasive imaging method we developed provides a useful screening tool for optimization of lymphatic targeting.

CONCLUSIONS

Our results show that the MW is inversely related to the rate of the loss of proteins from a SC injection site and proportionally related to the draining lymph node uptake in a mouse model. This investigation provides the first demonstration of this relationship in mice. *In vivo* fluorescence imaging provides a methodology useful for the optimization of protein targeting to the lymphatic circulation and for the study of the influence of the lymphatic system on drug bioavailability.

ACKNOWLEDGMENTS & DISCLOSURES

This work is supported by a grant from the University at Buffalo Center for Protein Therapeutics to MEM. SGB was supported in part by a fellowship from Pfizer Global Research and Development. We acknowledge the valuable assistance from Dr. Rajiv Kumar, Lisa A. Vathy, Dr. Hong Ding, and Dr. Ken-Tye Yong from the Institute for Lasers, Photonics and Biophotonics, University at Buffalo.

REFERENCES

1. Porter CJ, Edwards GA, Charman SA. Lymphatic transport of proteins after s.c. injection: implications of animal model selection. Adv Drug Deliv Rev. 2001;50:157–71.
2. Jung M, Lees P, Seewald W, King JN. Analytical determination and pharmacokinetics of robenacoxib in the dog. J Vet Pharmacol Ther. 2009;32:41–8.
3. Supersaxo A, Hein WR, Steffen H. Effect of molecular weight on the lymphatic absorption of water-soluble compounds following subcutaneous administration. Pharm Res. 1990;7:167–9.
4. Dreher MR, Liu W, Michelich CR, Dewhirst MW, Yuan F, Chilkoti A. Tumor vascular permeability, accumulation, and penetration of macromolecular drug carriers. J Natl Cancer Inst. 2006;98:335–44.
5. Kagan L, Gershkovich P, Mendelman A, Amsili S, Ezov N, Hoffman A. The role of the lymphatic system in subcutaneous absorption of macromolecules in the rat model. Eur J Pharm Biopharm. 2007;67:759–65.
6. Cubas R, Zhang S, Kwon S, Sevick-Muraca EM, Li M, Chen C, *et al.* Virus-like particle (VLP) lymphatic trafficking and immune response generation after immunization by different routes. J Immunother. 2009;32:118–28.
7. Ding H, Yong KT, Law WC, Roy I, Hu R, Wu F, *et al.* Non-invasive tumor detection in small animals using novel functional Pluronic nanomicelles conjugated with anti-mesothelin antibody. Nanoscale. 2011;3:1813–22.
8. Ding H, Yong KT, Roy I, Hu R, Wu F, Zhao L, *et al.* Bioconjugated PLGA-4-arm-PEG branched polymeric nanoparticles as novel tumor targeting carriers. Nanotechnology. 2011;22:165101.
9. Yong KT, Roy I, Ding H, Bergey EJ, Prasad PN. Biocompatible near-infrared quantum dots as ultrasensitive probes for long-term *in vivo* imaging applications. Small. 2009;5:1997–2004.
10. Yong K-T, Hu R, Roy I, Ding H, Vathy LA, Bergey EJ, *et al.* Tumor targeting and imaging in live animals with functionalized semiconductor quantum rods. ACS Appl Mater Interfaces. 2009;1:710–9.
11. Kwon S, Sevick-Muraca EM. Noninvasive quantitative imaging of lymph function in mice. Lymphat Res Biol. 2007;5:219–31.
12. Gearing AJH, Thorpe SJ, Miller K, Mangan M, Varley PG, Dudgeon T, *et al.* Selective cleavage of human IgG by the matrix metalloproteinases, matrilysin and stromelysin. Immunol Lett. 2002;81:41–8.
13. Plasencia MD, Isailovic D, Merenbloom SI, Mechref Y, Novotny MV, Clemmer DE. Resolving and assigning N-linked glycan structural isomers from ovalbumin by IMS-MS. J Am Soc Mass Spectrom. 2008;19:1706–15.
14. Bhansali SG, Balu-Iyer SV, Morris ME. Influence of route of administration and liposomal encapsulation on blood and lymph node exposure to the protein VEGF-C156S. J Pharm Sci. 2011.
15. Porter CJ, Charman SA. Lymphatic transport of proteins after subcutaneous administration. J Pharm Sci. 2000;89:297–310.
16. Hong H, Sun J, Cai W. Multimodality imaging of nitric oxide and nitric oxide synthases. Free Radic Biol Med. 2009;47:684–98.
17. Kim BS, Oh JM, Hyun H, Kim KS, Lee SH, Kim YH, *et al.* Insulin-loaded microcapsules for *in vivo* delivery. Mol Pharm. 2009;6:353–65.
18. Kim BS, Oh JM, Kim KS, Seo KS, Cho JS, Khang G, *et al.* BSA-FITC-loaded microcapsules for *in vivo* delivery. Biomaterials. 2009;30:902–9.
19. Wu F, Wuensch SA, Azadniv M, Ebrahimkhani MR, Crispe IN. Galactosylated LDL nanoparticles: a novel targeting delivery system to deliver antigen to macrophages and enhance antigen specific T cell responses. Mol Pharm. 2009;6:1506–17.
20. Lu ZR. Molecular imaging of HPMA copolymers: visualizing drug delivery in cell, mouse and man. Adv Drug Deliv Rev. 2010;62:246–57.
21. Erogbogbo F, Yong KT, Roy I, Hu R, Law WC, Zhao W, *et al. In vivo* targeted cancer imaging, sentinel lymph node mapping and multi-channel imaging with biocompatible silicon nanocrystals. ACS Nano. 2011;5:413–23.
22. Ballou B, Ernst LA, Andreko S, Harper T, Fitzpatrick JA, Waggoner AS, *et al.* Sentinel lymph node imaging using quantum dots in mouse tumor models. Bioconjug Chem. 2007;18:389–96.
23. Koyama Y, Talanov VS, Bernardo M, Hama Y, Regino CA, Brechbiel MW, *et al.* A dendrimer-based nanosized contrast agent dual-labeled for magnetic resonance and optical fluorescence imaging to localize the sentinel lymph node in mice. J Magn Reson Imaging. 2007;25:866–71.

24. Kim D, Lee ES, Park K, Kwon IC, Bae YH. Doxorubicin loaded pH-sensitive micelle: antitumoral efficacy against ovarian A2780/DOXR tumor. Pharm Res. 2008;25:2074–82.
25. Zou P, Xu S, Povoski SP, Wang A, Johnson MA, Martin Jr EW, *et al.* Near-infrared fluorescence labeled anti-TAG-72 monoclonal antibodies for tumor imaging in colorectal cancer xenograft mice. Mol Pharm. 2009;6:428–40.
26. Hu R, Yong KT, Roy I, Ding H, Law WC, Cai H, *et al.* Functionalized near-infrared quantum dots for *in vivo* tumor vasculature imaging. Nanotechnology. 2010;21:145105.
27. Diagaradjane P, Orenstein-Cardona JM, Colon-Casasnovas NE, Deorukhkar A, Shentu S, Kuno N, *et al.* Imaging epidermal growth factor receptor expression *in vivo*: pharmacokinetic and biodistribution characterization of a bioconjugated quantum dot nanoprobe. Clin Cancer Res. 2008;14:731–41.
28. Fox GB, Chin CL, Luo F, Day M, Cox BF. Translational neuroimaging of the CNS: novel pathways to drug development. Mol Interv. 2009;9:302–13.
29. Prajapati SI, Martinez CO, Bahadur AN, Wu IQ, Zheng W, Lechleiter JD, *et al.* Near-infrared imaging of injured tissue in living subjects using IR-820. Mol Imaging. 2009;8:45–54.
30. Koning GA, Krijger GC. Targeted multifunctional lipid-based nanocarriers for image-guided drug delivery. Anticancer Agents Med Chem. 2007;7:425–40.
31. Kumar R, Roy I, Ohulchanskky TY, Vathy LA, Bergey EJ, Sajjad M, *et al. In vivo* biodistribution and clearance studies using multimodal organically modified silica nanoparticles. ACS Nano. 2010;4:699–708.
32. Barrett T, Choyke PL, Kobayashi H. Imaging of the lymphatic system: new horizons. Contrast Media Mol Imaging. 2006;1:230–45.
33. Weissleder R. Scaling down imaging: molecular mapping of cancer in mice. Nat Rev Cancer. 2002;2:11–8.
34. Wang H, Chen K, Niu G, Chen X. Site-specifically biotinylated VEGF(121) for near-infrared fluorescence imaging of tumor angiogenesis. Mol Pharm. 2009;6:285–94.
35. Zou P, Xu S, Wang A, Povoski S, Johnson M, Martin E, et al. Near-infrared fluorescence labeled anti-TAG-72 monoclonal antibodies for tumor imaging in colorectal cancer xenograft mice. Mol Pharm. 2009.
36. Engeset A. The route of peripheral lymph to the blood stream; an x-ray study of the barrier theory. J Anat. 1959;93:96–100.
37. Kubik S. Anatomy of the lymphatic system. In: Foldi M, Foldi E, Kubik S, editors. Textbook of lymphology. San Francisco: Elsevier GmbH; 2003. p. 1–166.
38. Hildebrandt P. Subcutaneous absorption of insulin in insulin-dependent diabetic patients. Influence of species, physicochemical properties of insulin and physiological factors. Dan Med Bull. 1991;38:337–46.
39. Kang S, Brange J, Burch A, Volund A, Owens DR. Subcutaneous insulin absorption explained by insulin's physicochemical properties. Evidence from absorption studies of soluble human insulin and insulin analogues in humans. Diabetes Care. 1991;14:942–8.
40. Charman SA, McLennan DN, Edwards GA, Porter CJ. Lymphatic absorption is a significant contributor to the subcutaneous bioavailability of insulin in a sheep model. Pharm Res. 2001;18:1620–6.
41. Harvey AJ, Kaestner SA, Sutter DE, Harvey NG, Mikszta JA, Pettis RJ. Microneedle-based intradermal delivery enables rapid lymphatic uptake and distribution of protein drugs. Pharm Res. 2011;28:107–16.